Pulse-splitting in light propagation through N-type atomic media due to an interplay of Kerr-nonlinearity and group velocity dispersion

Rajitha K. V.,[1,*] Tarak N. Dey,[1,2,†] Jörg Evers,[2,‡] and Martin Kiffner[3,4,§]

[1] *Indian Institute of Technology Guwahati, Guwahati- 781 039, Assam, India*
[2] *Max-Planck-Institut für Kernphysik, Saupfercheckweg 1, 69117 Heidelberg, Germany*
[3] *Centre for Quantum Technologies, National University of Singapore, 3 Science Drive 2, Singapore 117543*[1]
[4] *Clarendon Laboratory, University of Oxford, Parks Road, Oxford OX1 3PU, United Kingdom*[2]

We investigate the spatio-temporal evolution of a Gaussian probe pulse propagating through a four-level N-type atomic medium. At two-photon resonance of probe-and control fields, weaker probe pulses may propagate through the medium with low absorption and pulse shape distortion. In contrast, we find that increasing the probe pulse intensity leads to a splitting of the initially Gaussian pulse into a sequence of subpulses in the time domain. The number of subpulses arising throughout the propagation can be controlled via a suitable choice of the probe and control field parameters. Employing a simple theoretical model for the nonlinear pulse propagation, we conclude that the splitting occurs due to an interplay of Kerr nonlinearity and group velocity dispersion.

PACS numbers: 42.50.Gy, 32.80.Qk, 42.65.-k

I. INTRODUCTION

Atomic coherence and quantum interference effects are key drivers for the control of light-matter interactions. Among the most prominent effects are electromagnetically induced transparency (EIT) [1, 2] and related phenomena like the slowing and stopping of light [3–7], the coherent storage and retrieval of light [8–11], and stationary light [12–21]. EIT can also be used to enhance the nonlinear susceptibility [1, 22–25]. However, conventional EIT schemes are limited in their enhancement of nonlinear effects due to the presence of considerable absorption [1, 26]. Multilevel EIT-related atomic systems are a possible route to circumvent these limitations. In this spirit, Schmidt and Imamŏglu proposed a four-level N-configuration system in which the standard EIT level scheme is augmented by an additional off-resonantly-driven transition for the enhancement of the Kerr-nonlinearity [26]. This Kerr-nonlinearity was experimentally observed in [27] and has many interesting applications. For example, the N-type level system has been shown to exhibit cross-Kerr interactions [28] as well as the phenomena of optical bistability [29] and optical switching [30] in cavity systems and hollow-core optical fibres [31]. On the quantum level, the N-level system gives rise to nonlinear optical interactions that can be conservative [35] or dissipative [38]. These two-particle interactions were employed for the realization of strongly correlated polariton systems [32–34].

From a practical point of view, it is important to measure the effect of the Kerr-nonlinearity on the probe field. An obvious and common way of probing an optical system is by studying its response to an optical pulse. In particular, the polariton systems in [32–34] involve a sequence where an input pulse is stored, processed and then released for readout. An evident question is thus how the Kerr-nonlinearity in the N-level system modifies the propagation of a weak, classical probe pulse. However, up to now this problem has not received much attention [36, 37].

Motivated by this, here, we investigate the pulse propagation through a coherent medium in N-type configuration, see Fig. 1. We solve the Maxwell-Bloch equations governing the propagation dynamics numerically and consider resonant driving of the Raman transition within the Λ sub-system. As a first result, we find that a weak probe may propagate through the medium with low absorption and pulse shape distortion, provided that the Kerr detuning of the probe field is sufficiently large. However, at stronger probe pulse intensities, the numerical simulations predict a splitting of the initially Gaussian pulse into sub-pulses, which subsequently propagate through the medium without further splittings. To interpret these results, we derive a simple analytical model for nonlinear pulse propagation through the N-type medium. From this model, we conclude that the pulse splitting is a direct manifestation of the self-phase modulation associated with the Kerr nonlinearity in the presence of group velocity dispersion. The group velocity dispersion can be adjusted via the detuning of the probe and control fields with respect to the excited state of the Λ sub-system. Measuring the temporal pulse shape of the probe pulse at the output thus indicates the strength of the Kerr nonlinearity experienced inside the medium. A similar pulse splitting phenomenon should be observable in other systems with EIT-enhanced nonlinearities giving rise to self-phase modulation effects. For example, EIT in Rydberg systems [39] can give rise to giant photon non-linearities mediated by the interaction between the Rydberg atoms [40–42].

This paper is organized as follows. In Sec. II we intro-

*Electronic address: rajitha@iitg.ac.in
†Electronic address: tarak.dey@iitg.ernet.in
‡Electronic address: jorg.evers@mpi-hd.mpg.de
§Electronic address: martin.kiffner@physics.ox.ac.uk

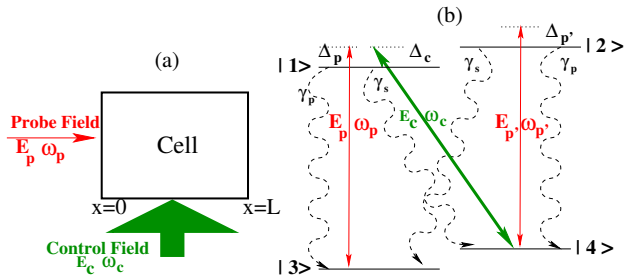

FIG. 1: (Color online) (a) A block diagram of the system of interest. We assume that the control field intensity is constant along the propagation direction. (b) Schematic representation of four-level atoms in N-type configuration. We consider two $J = 1/2$ Zeeman manifolds with excited states $|1\rangle = |m_e = -1/2\rangle$ and $|2\rangle = |m_e = 1/2\rangle$ and ground states $|3\rangle = |m_g = -1/2\rangle$ and $|4\rangle = |m_g = 1/2\rangle$. The σ^--polarized control field $\boldsymbol{E}_c$ couples to the transition $|1\rangle \leftrightarrow |4\rangle$, and the π-polarized probe field $\boldsymbol{E}_p$ interacts with the $|1\rangle \rightarrow |3\rangle$ and $|2\rangle \rightarrow |4\rangle$ transitions.

duce the Maxwell-Bloch equations governing the pulse propagation in the considered atomic four-level medium. In Sec. III, the propagation dynamics of the pulse is studied numerically at different parameter conditions. In order to find a qualitative interpretation of our numerical findings, we introduce a model for the description of pulse propagation in nonlinear media in Sec. IV. Section V provides a summary and discussion of our results.

II. THEORETICAL MODEL

We consider a homogeneous atomic medium interacting with two laser fields as shown in Fig. 1(a). The weak probe and the strong control fields propagate in perpendicular directions. The atomic four-level system in N-type configuration is depicted in Fig. 1(b). In the following, we assume that this level scheme is realized with two $J = 1/2$ Zeeman manifolds via polarization selection. The weak probe field with central frequency ω_p couples to the π-transitions $[|1\rangle \leftrightarrow |3\rangle$ and $|2\rangle \leftrightarrow |4\rangle]$ and is defined as

$$\boldsymbol{E}_p(t) = \boldsymbol{e}_\pi \mathcal{E}_p e^{i(k_p x - \omega_p t)} + \text{c.c.}, \tag{1}$$

where $\boldsymbol{e}_\pi$ is the polarization unit vector, $k_p = \omega_p/c$ and c is the speed of light. The strong σ^--polarized control field with frequency ω_c couples to the $|1\rangle \leftrightarrow |4\rangle$ transition and can be written as

$$\boldsymbol{E}_c(t) = \boldsymbol{e}_{\sigma^-} \mathcal{E}_c e^{i(k_c z - \omega_c t)} + \text{c.c.}, \tag{2}$$

where $k_c = \omega_c/c$. In electric-dipole and rotating-wave approximation, the semiclassical Hamiltonian of the system is

$$\begin{aligned} H_{\text{int}} &= -\hbar(\Delta_P - \Delta_C)|4\rangle\langle 4| - \hbar\Delta_P|1\rangle\langle 1| \\ &- \hbar(\Delta_P + \Delta_{P'} - \Delta_C)|2\rangle\langle 2| \\ &- [(|2\rangle\langle 4| - |1\rangle\langle 3|)\Omega_p + |1\rangle\langle 4|\Omega_c + \text{H.c.}] \,. \end{aligned} \tag{3}$$

The Rabi frequencies of the probe and control fields in Eq. (3) are defined as

$$\Omega_p = \frac{\boldsymbol{d}_{24} \cdot \boldsymbol{e}_\pi}{\hbar} \mathcal{E}_p \,, \tag{4a}$$

$$\Omega_c = \frac{\boldsymbol{d}_{14} \cdot \boldsymbol{e}_{\sigma^-}}{\hbar} \mathcal{E}_c \,, \tag{4b}$$

where $\boldsymbol{d}_{ij}$ is the electric dipole moment for the transition between levels $|i\rangle$ and $|j\rangle$. Note that $\boldsymbol{d}_{24} = -\boldsymbol{d}_{13}$ according to the Clebsch-Gordan coefficients of the considered $J = 1/2 \leftrightarrow J = 1/2$ level scheme. The detunings of probe and control fields are given by

$$\Delta_P = \omega_p - \omega_{13} \,, \tag{5a}$$

$$\Delta_{P'} = \omega_p - \omega_{24} \,, \tag{5b}$$

$$\Delta_C = \omega_c - \omega_{14} \,. \tag{5c}$$

We model the quantum dynamics of the atoms using the master equation approach. The matrix elements of the atomic density operator ρ obey the following equations,

$$\begin{aligned} \dot{\rho}_{11} &= -(\gamma_p + \gamma_s)\rho_{11} - i\Omega_p\rho_{31} + i\Omega_p^*\rho_{13} \\ &+ i\Omega_c\rho_{41} - i\Omega_c^*\rho_{14} \,, \end{aligned} \tag{6a}$$

$$\begin{aligned} \dot{\rho}_{12} &= -[\gamma_p + \gamma_s - i(\Delta_C - \Delta_{P'})]\rho_{12} + i\Omega_c\rho_{42} \\ &- i\Omega_p\rho_{32} - i\Omega_p^*\rho_{14}, \end{aligned} \tag{6b}$$

$$\begin{aligned} \dot{\rho}_{13} &= -[(\gamma_p + \gamma_s)/2 - i\Delta_P]\rho_{13} + i\Omega_c\rho_{43} \\ &- i\Omega_p(\rho_{33} - \rho_{11}), \end{aligned} \tag{6c}$$

$$\begin{aligned} \dot{\rho}_{14} &= -[(\gamma_p + \gamma_s)/2 - i\Delta_C]\rho_{14} - i\Omega_p(\rho_{34} + \rho_{12}) \\ &+ i\Omega_c(\rho_{44} - \rho_{11}), \end{aligned} \tag{6d}$$

$$\dot{\rho}_{22} = -(\gamma_p + \gamma_s)\rho_{22} + i\Omega_p\rho_{42} - i\Omega_p^*\rho_{24} \,, \tag{6e}$$

$$\begin{aligned} \dot{\rho}_{23} &= -\left[(\gamma_p + \gamma_s)/2 + i(\Delta_C - (\Delta_P + \Delta_{P'}))\right]\rho_{23} \\ &+ i\Omega_p\rho_{43} + i\Omega_p\rho_{21} \,, \end{aligned} \tag{6f}$$

$$\begin{aligned} \dot{\rho}_{24} &= -\left[(\gamma_p + \gamma_s)/2 - i\Delta_{P'}\right]\rho_{24} + i\Omega_p(\rho_{44} - \rho_{22}) \\ &- i\Omega_c\rho_{21} \,, \end{aligned} \tag{6g}$$

$$\dot{\rho}_{33} = \gamma_p\rho_{11} + \gamma_s\rho_{22} - i\Omega_p^*\rho_{13} + i\Omega_p\rho_{31} \,, \tag{6h}$$

$$\begin{aligned} \dot{\rho}_{34} &= [\Gamma + i(\Delta_P - \Delta_C)]\,\rho_{34} - i\Omega_p^*\rho_{14} \\ &- i\Omega_p\rho_{32} - i\Omega_c\rho_{31}, \end{aligned} \tag{6i}$$

where γ_p $[\gamma_s]$ is the decay rate of the π $[\sigma]$ transition. These decay constants are related through the Clebsch-Gordan coefficients of the level scheme and obey $\gamma_s = 2\gamma_p = 2\gamma/3$, where γ is the total decay rate of each excited state. The decay rate of the ground state coherence is denoted by Γ. The medium polarization induced by the probe field can be expressed in terms of the off-diagonal density matrix elements ρ_{13} and ρ_{24} as

$$\boldsymbol{P} = \mathcal{N}(\boldsymbol{d}_{31}\rho_{13} + \boldsymbol{d}_{42}\rho_{24}) \,, \tag{7}$$

where $\mathcal{N}$ is the number density of the medium. The spatio-temporal evolution of the probe pulse through the medium is governed by Maxwell's equations. In the slowly varying envelope approximation, we find

$$\left(\frac{\partial}{\partial x} + \frac{1}{c}\frac{\partial}{\partial t}\right)\Omega_p = i\eta\,(\rho_{24} - \rho_{13}) \,, \tag{8}$$

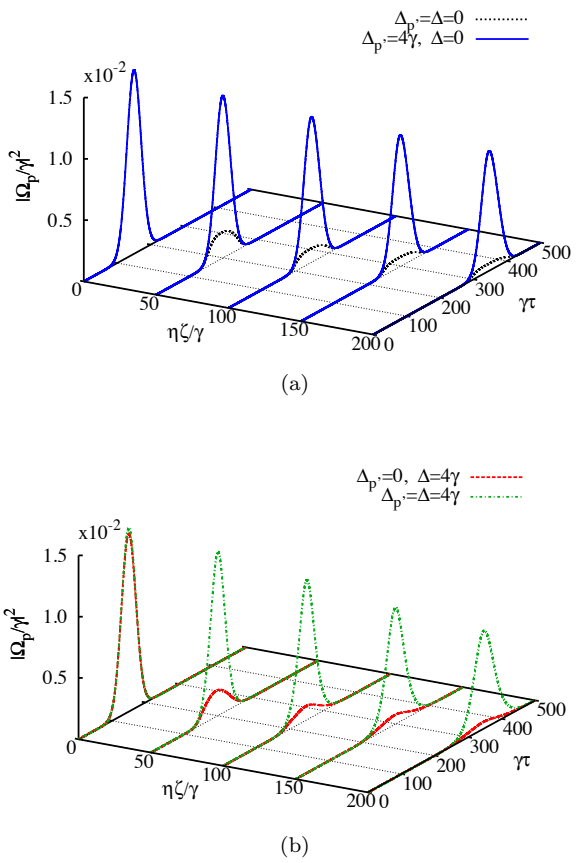

FIG. 2: (Color online) Intensity $|\Omega_p/\gamma|^2$ of a weak probe pulse as a function of position and time for different detuning conditions. The parameters in (a) and (b) are $\Omega_c = \gamma$, $\Omega_p = \sqrt{0.015}\gamma$, $\sigma_p = 30/\gamma$, and $\Gamma = 0$.

where

$$\eta = \gamma \frac{\mathcal{N}\lambda^2}{8\pi} \tag{9}$$

is the coupling constant and λ is the wavelength of the transition $|1\rangle \leftrightarrow |3\rangle$.

In order to facilitate the numerical integration of the coupled Maxwell-Bloch equations in Eqs. (6) and (8), we introduce a co-moving coordinate system

$$\tau = t - \frac{x}{c}, \qquad \zeta = x. \tag{10}$$

This change of coordinates reduces the partial differential equation in Eq. (8) to an ordinary differential equation with respect to the independent variable ζ,

$$\frac{\partial \Omega_p}{\partial \zeta} = i\eta\,(\rho_{24} - \rho_{13})\,. \tag{11}$$

Typical parameter values are $\mathcal{N} = 5\times10^{11}\text{atoms/cm}^3$, $\lambda = 780$ nm, and $\gamma = 2\pi \times 10^6$ Hz. Throughout this paper we assume that the depletion of the strong control field throughout its propagation can be neglected such

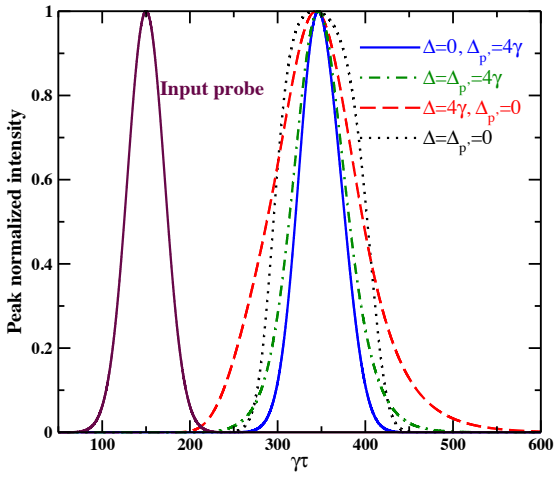

FIG. 3: (Color online) Probe pulse intensities at the medium exit at $\eta\zeta/\gamma = 200$. Parameters are as in Fig. 2. To facilitate the analysis of the pulse widths, all pulses are shown normalized to their respective peak values.

that its intensity is independent of position. We further choose values of Δ_P and Δ_C compatible with the resonant Raman condition $\Delta_P = \Delta_C$, and hence we define

$$\Delta = \Delta_P = \Delta_C\,. \tag{12}$$

III. NUMERICAL ANALYSIS

We start our discussion with a numerical analysis of the probe field propagation through the atomic four-level medium. To this end, we assume that the shape of the input pulse at the medium boundary at $\zeta = 0$ is given by

$$\Omega_p(\zeta = 0, \tau) = \Omega_p^0 e^{-\frac{(\tau-\tau_0)^2}{2\sigma_p^2}}, \tag{13}$$

where Ω_p^0 and σ_p are the amplitude and temporal width of the Gaussian pulse, respectively. Furthermore, all atoms are assumed to be in the ground state $|3\rangle$ initially.

Our choice of parameters is guided by the following considerations. For suitable parameters, the N-type level scheme gives rise to self-phase modulation (SPM) due to the optical Kerr effect [26, 43]. As a consequence, the probe field experiences an intensity-dependent refractive index and thus acquires a time-dependent phase shift in accordance with its temporal intensity profile. This time-varying phase can be interpreted as a transient frequency shift. Furthermore, if the intensity of the probe pulse is sufficiently large, the SPM gives rise to characteristic modification of its Fourier spectrum. For example, an initially Gaussian Fourier spectrum typically break up into several peaks in the Fourier domain [43].

A. Weak probe pulses

In a first step we focus on weak probe pulses such that the effect of SPM is negligible. To this end, we evaluate the Fourier spectra inside the medium and verify that typical manifestations of SPM are absent. In this parameter regime the remaining system parameters governing the probe pulse propagation are given by Δ and Δ_C. In the following we discuss four different detuning conditions in order to systematically investigate the influence of the Raman detuning Δ and Kerr detuning $\Delta_{P'}$. For this, we evaluate all four combinations of Δ and $\Delta_{P'}$ being either 0 or 4γ:

$$\begin{aligned}
&(i) && \Delta = 0 && \text{and} && \Delta_{P'} = 4\gamma\,,\\
&(ii) && \Delta = 4\gamma && \text{and} && \Delta_{P'} = 4\gamma\,,\\
&(iii) && \Delta = 0 && \text{and} && \Delta_{P'} = 0\,,\\
&(iv) && \Delta = 4\gamma && \text{and} && \Delta_{P'} = 0\,.
\end{aligned}$$

The resulting pulse propagation dynamics is shown in Fig. 2. It can be seen that $\Delta_{P'}$ crucially affects the absorption. The two cases with $\Delta_{P'} = 0$ lead to a transmission of less than 10% of the probe pulse intensity through the medium. In contrast, the cases $\Delta_{P'} = 4\gamma$ give rise to approximately 75% probe intensity transmission. This behavior can be traced back to the absorption on the $|4\rangle \leftrightarrow |2\rangle$ transition. Figure 3 shows the effect of Δ, which affects the shape and width of the transmitted pulse, whereas its effect on the transmitted intensity is small.

B. Strong probe pulses

Next, we consider probe pulses with higher intensities such that the effect of SPM is expected to become of relevance. Figure 4 shows the probe pulse propagation dynamics as function of the propagation distance for case (ii), i.e., $\Delta_{P'} = \Delta = 4\gamma$. The other parameters are chosen as in Figs. 2 and 3, except for the intensity higher by a factor of 10. Panel (a) shows the temporal probe pulse shape throughout the propagation. We find that the pulse gradually breaks up, until two fully separated pulses are obtained at $\eta\zeta/\gamma = 100$. The shapes of these sub-pulses remain Gaussian, and they are found to subsequently propagate through the medium without further break-up. However, the individual subpulses broaden as they propagate through the medium, as it was also found in the corresponding weak probe pulse case of Fig. 2.

To further analyze this pulse break-up, Fig. 4(b) shows the power spectra of the probe pulse throughout its propagation, obtained by Fourier transformation of the temporal pulse shape. The power spectrum evolves from the Gaussian input spectrum into a double-peaked structure which is a characteristic signature of the SPM effect.

A further numerical study reveals that the number of generated subpulses depends on the initial probe field intensity. Figure 5 demonstrates that a three-peak pulse

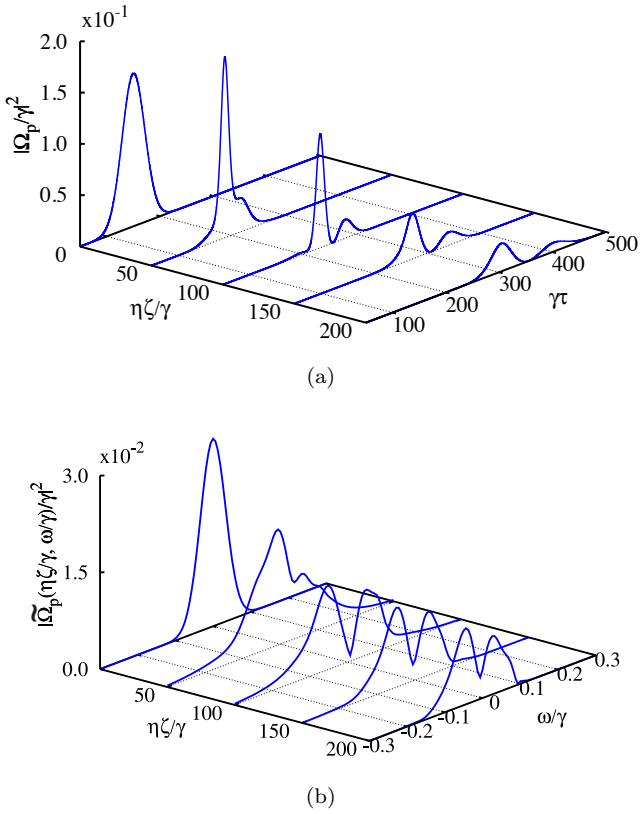

FIG. 4: (Color online) (a) Intensity $|\Omega_p/\gamma|^2$ of a stronger probe pulse as function of the propagation distance. Parameters are $\Delta = \Delta_{P'} = 4\gamma$ and $\Omega_p = \sqrt{0.15}\gamma$; all other parameters are chosen as in Fig. 2. (b) shows the corresponding probe pulse power spectra obtained by Fourier transformation as function of the propagation distance.

can be generated from a single Gaussian probe pulse if the initial probe field intensity is suitably increased. As expected, the precise shape of the output pulse depends sensitively on the probe pulse intensity and the value of the detuning Δ. For example, the three-peak shape in Fig. 5 turns into a two-peak structure if the three-photon detuning is increased to $\Delta_{P'} = \Delta = 8\gamma$. Finally, we verified that the shaping and splitting of the probe pulse does not rely on the initial Gaussian pulse shape and can also be observed with non-Gaussian initial pulse shapes, such as secant-hyperbolic pulses.

IV. THEORETICAL ANALYSIS

Next, we provide a theoretical interpretation of the numerical results presented in Sec. III. To this end, we adapt the standard description of pulse propagation in optical fibers [43] to our system.

We find that this model reproduces our numerical results accurately for weak probe pulses where the SPM phenomenon is small. For parameters where the SPM effect becomes dominant our model allows us to gain qual-

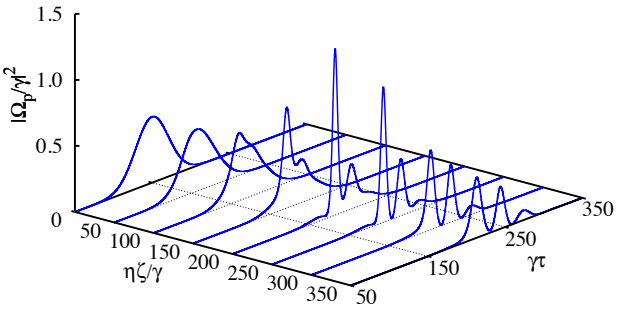

FIG. 5: (Color online) Propagation dynamics of a probe pulse with $\Omega_p = \sqrt{0.5}\gamma$ and $\Delta = \Delta_{P'} = 4\gamma$. All other parameters are chosen as in Fig. 2.

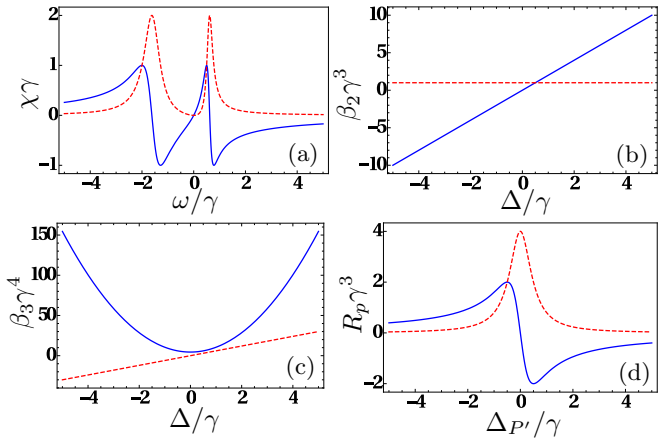

FIG. 6: (Color online) (a) Real and imaginary parts of the linear susceptibility χ in Eq. (A12) as a function of the Fourier component ω of the probe pulse envelope. We have $\beta_0 = \chi(0) = 0$, and β_n is the nth derivative of χ at $\omega = 0$, see Appendix A. The real and imaginary parts of β_2 [β_3] are shown in (b) [(c)]. (d) Real and imaginary parts of R_p as a function of the Kerr detuning $\Delta_{p'}$ for $\Delta = 4\gamma$. In (a)-(d), blue solid (red dashed) lines show real (imaginary) parts and $\Omega_c = \gamma$.

itative insights and provides an intuitive explanation for the pulse splitting phenomenon described in Sec. III.

Details on our simple model for the propagation of optical pulses in nonlinear media inspired by the standard fiber optics approach [43] are provided in Appendix A. There, we perform a perturbative analysis with respect to the probe field strength to derive the linear susceptibility $\chi(\omega)$ of the probe field, and find that the spatio-temporal evolution of the probe pulse can be described by

$$\left(\frac{\partial}{\partial x} + \frac{1}{c}\frac{\partial}{\partial t}\right)\Omega_p = i\eta\left(\sum_{n=0}^{3}\beta_n\frac{i^n}{n!}\frac{\partial^n\Omega_p}{\partial t^n}\right) + i\eta R_p\left|\Omega_p\right|^2\Omega_p\,. \tag{14}$$

The parameters β_n and R_p are determined by the microscopic model introduced in Sec. II. In particular,

$$\beta_n = \left.\frac{\partial^n\chi}{\partial\omega^n}\right|_{\Delta_P=\Delta_C}^{\omega=0} \tag{15}$$

is the n-th derivative of the medium susceptibility $\chi(\omega)$ evaluated at the center frequency $\omega = 0$ of the probe pulse [see Eq. (A13)]. Note that due to the approximations used throughout the derivation, our model described by Eq. (14) is valid under the following conditions. (α) The probe pulse must be sufficiently long in time such that the atomic medium follows the probe pulse dynamics adiabatically. (β) The probe field spectrum must be sufficiently narrow such that the Taylor expansion of the linear susceptibility is justified [see Appendix A for details]. (γ) The probe field intensity must be weak enough such that all non-linear effects are well described by the third-order term proportional to R_p.

We start by analyzing the relevant model parameters, see Fig. 6. Panel (a) shows the linear susceptibility $\chi(\omega)$ as a function of frequency ω scanned across the probe pulse center frequency $\omega = 0$ [see Eq. (A9)]. The parameter β_0 is the linear susceptibility χ of the probe field evaluated at $\omega = 0$, and vanishes for resonant Raman fields [see Eq. (12)] if the ground-state decoherence rate Γ is neglected. β_1 is related to the group velocity of the pulse via

$$v_g = [1/c + \eta\mathrm{Re}(\beta_1)]^{-1}, \tag{16}$$

where Re denotes the real part. The parameters β_2 and β_3 account for group velocity dispersion. The real and imaginary parts of β_2 [β_3] are shown in Fig. 6(b) [(c)] as a function of the detuning Δ. Both real and imaginary parts of β_2 and β_3 determine the width and amplitude of the probe pulse at the output. For $\Delta = 0$ only the imaginary part of β_2 is different from zero. This term accounts for absorption due to the finite width of the EIT window in frequency space. For larger values of Δ the real part of β_2 increases and describes the change of the group velocity for frequencies away from the central frequency of the pulse. In general, β_3 represents a higher-order correction to the group velocity dispersion. The nonlinearity due to the Kerr transition is proportional to R_p defined in Eq. (A8), and the dependence of R_p on $\Delta_{P'}$ is shown in Fig. 6(d). The imaginary part of R_p is only large for $\Delta_{P'} \approx 0$, and hence absorption on the Kerr transition is small for $\Delta_{P'}/\gamma \gg 1$. Note that the quantitative impact of the term proportional to R_p in Eq. (14) depends on the probe pulse intensity.

Equation (14) can be numerically solved using the split-step Fourier method [43]. We find excellent agreement with the numerical results obtained in Sec. III for parameters where the model conditions (α)-(γ) are met. In particular, this is the case for all parameters where the SPM effect is small, and in this regime the explanation of all phenomena in terms of the parameters β_i and R_p is straightforward. We begin with a weak probe pulse and a large detuning $\Delta_{P'}$ on the Kerr transition [cases (i) and (ii) in Sec. III]. Since the imaginary part of R_p

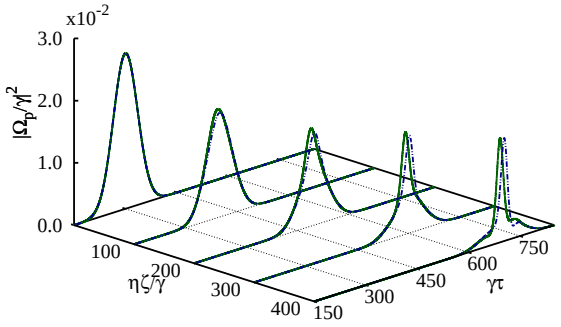

(a)

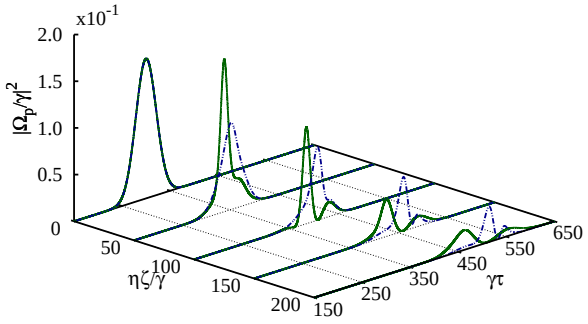

(b)

FIG. 7: (Color online) Comparison between the full numerical solution to Eqs. (6) and (8) [green solid line] and the simple model in Eq. (14) [blue dot-dashed line]. The parameters in (a) are $\Omega_p = 0.025\gamma$, $\sigma_p = 50/\gamma$, $\Delta = \gamma$ and $\Delta_{P'} = 3\gamma$.. Results in (b) correspond to $\Omega_p = \sqrt{0.15}\gamma$, $\sigma_p = 30/\gamma$, and $\Delta = \Delta_{P'} = 4\gamma$.

is small and hence the absorption on the Kerr transition is small for these parameters, the probe pulse can propagate through the medium without significant losses. The additional broadening of the probe pulse in case (ii) as compared to (i) can be explained by the non-zero group velocity dispersion for the parameters in (ii). Next we consider a resonant Kerr field $\Delta_{P'} = 0$ [cases (iii) and (iv) in Sec. III]. The strong damping of the probe pulse found in Sec. III can be explained by the large imaginary part of R_p. The Kerr transition hence destroys the EIT phenomenon and leads to absorption of the the probe pulse. The non-vanishing group velocity dispersion in case (iv) leads to an additional broadening of the pulse as compared to (iii).

In order to gain a qualitative insight into the pulse splitting phenomenon discussed in Sec.III B, we identify a parameter regime where the pulse splitting occurs and the conditions (α, β, γ) of our model are met. This is shown in Fig. 7(a), where the pulse starts splitting at the end of the medium, and there is a reasonable agreement between the full numerical calculations and our theoretical model. From the model, the pulse splitting effect can be understood as follows. The SPM associated with R_p results in a splitting of the probe pulse in frequency space. In the presence of group velocity dispersion described by β_2 and β_3, these pulses propagate at different speeds. This explains the emergence of two different pulses in the temporal domain.

The pulse splitting as shown in Fig. 4 is much more pronounced than in Fig. 7. Our model predicts the pulse splitting effect for the parameters in Fig. 4, but it is not sufficient for reproducing quantitatively correct results. This is shown in Fig. 7(b), where we compare the theoretical model to the full numerical simulation for parameters as in Fig. 4(a). The reason for the discrepancy between the simple model in Eq. (14) and the numerical approach is that the conditions (α)-(γ) for the validity of the model are not met for the considered parameters. In particular, the probe pulse width in frequency space is not narrow enough to justify the adiabatic approximation rigorously. Second, the linear susceptibility χ varies too strongly over the width of the pulse in frequency space for $\Delta = 4\gamma$ such that the expansion of χ up to third order is insufficient. Third, the probe pulse intensity is not small enough such that higher order terms beyond the third-order nonlinearity will contribute.

Despite these shortcomings, we find that the qualitative explanation for the pulse splitting effect suggested by the simple model remains valid. To this end, we note that the power spectrum in Fig. 4(b) found by numerically fourier transforming the data in Fig. 4(a) shows a clear signature of the SPM effect. The initially Gaussian pulse develops into two separate sub-pulses with increasing propagation distance. Let us denote the central frequencies of these pulses by ω_+ and ω_-, respectively. From the data in Fig. 4(b) we find $\omega_\pm \approx \pm 0.05\gamma$. Next we show that the splitting of the probe pulses in the temporal domain is associated with the different group velocities $v_g(\omega_\pm)$ of these two sub-pulses. In order to verify this, we calculate $v_g(\omega_\pm)$ from the dispersion relation shown in Fig. 6(a) according to Eq. (16) with β_1 evaluated at $\omega = \omega_\pm$. As can be seen from Fig. 4(b), the two-pulse structure starts to develop at $\eta\zeta/\gamma \approx 50$ and is fully established at $\eta\zeta/\gamma \approx 100$. We thus assume that the two sub-pulses evolve over a distance $\eta\Delta\zeta/\gamma \approx 130$ with different group velocities until the end of the medium at $\eta\zeta/\gamma = 200$ is reached. We estimate that the corresponding time difference is $130\gamma/\eta|1/v_g(\omega_-) - 1/v_g(\omega_+)| \approx 90/\gamma$, which is in reasonable agreement with the time delay at $\eta\zeta/\gamma = 200$ according to Fig. 4(a). In conclusion, we find that the pulse splitting arises from an interplay between SPM and group velocity dispersion.

Finally, we note that the pulse splitting reduces the in-

tensity of the individual pulses, and suppresses nonlinear effects. Hence, the two pulses in Fig. 4(a) do not split again. Higher intensities such as in Fig. 5 lead to three pulses in the temporal domain. Interestingly, this result does not agree with the naive expectation that the pulse first breaks up in two pulses that subsequently split up in two pulses each, giving rise to a total of four pulses. This outcome is a manifestation of the non-linearity of the SPM phenomenon.

V. CONCLUSION

We have studied the propagation dynamics of a Gaussian pulse through an atomic medium in four-level N-type configuration under different input conditions of control and probe field intensities and detunings. As our first result, we have found that at two-photon resonance condition with large Kerr detuning, distortionless propagation of the probe pulse with low absorption is possible. In contrast, when the intensity of the probe pulse becomes higher, a splitting of the single Gaussian input pulse into a sequence of pulses may occur. To interpret the origin of this pulse splitting, we have derived a simple theoretical model for nonlinear pulse propagation in our model system. The parameters of this model can be calculated from the system's steady state density matrix. We conclude that in particular an interplay between Kerr nonlinearity and group velocity dispersion leads to the pulse splitting. The nonlinearity leads to a decomposition of the probe pulse in frequency space. Subsequently, the such formed subpulses propagate with different velocity due to group velocity dispersion, such that a splitting in the time domain arises. The temporal shape of the probe pulse at the output does thus indicate the strength of the self-phase modulation induced by the Kerr-nonlinearity. Our numerical analysis has shown that the number of peaks can be controlled by adjusting the laser parameters. For example, the group velocity can be controlled by the detuning of the probe and control fields with the excited state of the Λ sub-system. In addition, the Kerr-detuning and the laser intensities control the magnitude of the self-phase modulation.

VI. ACKNOWLEDGMENTS

MK thanks the National Research Foundation and the Ministry of Education of Singapore for support.

Appendix A: Model parameters

Here we outline the derivation of the model in Eq. (14) from Eqs. (6) and (8). We assume that the probe field is sufficiently weak ($|\Omega_p| \ll \gamma$, $|\Omega_c|$) and pursue the perturbative approach outlined in [44, 45]. The atomic density operator is expanded as

$$\rho = \sum_{k=0}^{\infty} \rho^{(k)}, \tag{A1}$$

where $\rho^{(k)}$ denotes the contribution to ρ in kth order in the probe field Hamiltonian

$$H_p = -(|2\rangle\langle 4| - |1\rangle\langle 3|)\Omega_p + \text{H.c.}\,. \tag{A2}$$

In order to obtain the solutions $\rho^{(k)}$ we re-write the master equation (6) as

$$\mathcal{L}\rho = \mathcal{L}_0\rho - \frac{i}{\hbar}[H_p, \rho]\,, \tag{A3}$$

where the linear super-operator $\mathcal{L}_0$ is independent of the probe field. Inserting the expansion (A1) into Eq. (A3) leads to the following set of coupled differential equations

$$\dot{\rho^{(0)}} = \mathcal{L}_0\rho^{(0)}\,, \tag{A4}$$

$$\dot{\rho^{(k)}} = \mathcal{L}_0\rho^{(k)} - \frac{i}{\hbar}[H_p, \rho^{(k-1)}], \quad k > 0. \tag{A5}$$

Equation (A4) describes the interaction of the atom with the control field to all orders and in the absence of the probe field. Higher-order contributions to ρ can be obtained if Eq. (A5) is solved iteratively. Equations (A4) and (A5) must be solved under the constraints $\text{Tr}(\rho^{(0)}) = 1$ and $\text{Tr}(\rho^{(k)}) = 0$ $(k > 0)$.

First we consider the nonlinear term where we employ the adiabatic approximation, i.e., we assume that the temporal length of the probe pulse is much longer than the lifetime of the excited states. In this case we can find the nonlinear response of the medium to the probe field by solving for the steady state of Eqs. (A4) and (A5) up to third order in H_p and obtain

$$\rho^{(0)} = |3\rangle\langle 3|\,. \tag{A6}$$

Under the resonance condition $\Delta = \Delta_P = \Delta_C$ the only non-zero terms contributing in Eq. (8) are $\rho_{24}^{(3)}$ and $\rho_{13}^{(3)}$. We find

$$\rho_{24}^{(3)} - \rho_{13}^{(3)} = R_p|\Omega_p|^2\Omega_p\,, \tag{A7}$$

where

$$R_p = -\frac{2}{(\Delta_{P'} + i\gamma/2)|\Omega_c|^2}\,. \tag{A8}$$

Next we calculate the dominant correction arising from the spread of the probe pulse in frequency space. To this end we consider the Fourier expansion of the slowly varying probe pulse envelope,

$$\Omega_p(t) = \int_{-\infty}^{\infty} \tilde{\Omega}_p(\omega)e^{-i\omega t}\mathrm{d}\omega\,. \tag{A9}$$

We solve Eqs. (A4) and (A5) up to first order and obtain

$$\rho_{13}^{(1)}(t) = -\int_{-\infty}^{\infty} \chi(\omega)\tilde{\Omega}_p(\omega)e^{-i\omega t}\mathrm{d}\omega\,, \tag{A10}$$

where

$$\chi(\omega) = -\frac{\omega + \Delta_P - \Delta_C}{(\omega + \Delta_P + i\gamma/2)(\omega + \Delta_P - \Delta_C) - |\Omega_c|^2}\,. \tag{A11}$$

There are no other terms up to first order contributing to the coherences ρ_{13} or ρ_{24}, and χ is shown in Fig. 5. If χ is slowly varying over the typical width of the probe pulse, we can expand χ in a Taylor series around $\omega = 0$. For $\Delta_P = \Delta_C = \Delta$ and up to third order we obtain

$$\chi(\omega) \approx \sum_{n=0}^{3} \frac{\omega^n}{n!}\beta_n\,, \tag{A12}$$

where

$$\beta_n = \left.\frac{\partial^n \chi}{\partial \omega^n}\right|_{\Delta_P=\Delta_C}^{\omega=0}\,. \tag{A13}$$

The coefficients β_k are shown in Fig. 6 and given by

$$\beta_0 = 0\,, \tag{A14}$$

$$\beta_1 = \frac{1}{|\Omega_c|^2}\,, \tag{A15}$$

$$\beta_2 = \frac{2(\Delta + i\gamma/2)}{|\Omega_c|^4}\,, \tag{A16}$$

$$\beta_3 = \frac{6[|\Omega_c|^2 + (\Delta + i\gamma/2)^2]}{|\Omega_c|^6}\,. \tag{A17}$$

Inserting the expansion (A12) into Eq. (A10) gives

$$\rho_{13}^{(1)}(t) \approx -\sum_{n=0}^{3} \beta_n \frac{i^n}{n!}\frac{\partial^n \Omega_p}{\partial t^n}. \tag{A18}$$

In summary, the right-hand side of Eq. (8) can be written as

$$i\eta(\rho_{24} - \rho_{13}) \approx i\eta\left[\rho_{24}^{(3)} - \rho_{13}^{(3)} - \rho_{13}^{(1)}\right]\,. \tag{A19}$$

Substituting the results from Eqs. (A7) and (A18) into Eq. (A19) allows us to obtain Eq. (14).

[1] M. Fleischhauer, A. Imamoglu, J.P. Marangos, Rev. Mod. Phys. **77**, 633 (2005).
[2] S. E. Harris, Phys. Today **50**(7), 36(1997).
[3] L. V. Hau, S. E. Harris, Z. Dutton and C. H. Behroozi, Nature (London) **397**, 594 (1999).
[4] M. M. Kash, V. A. Sautenkov, A. S. Zibrov, L. Hollberg, G. R. Welch, M. D. Lukin, Y. Rostovtsev, E. S. Fry, and M. O. Scully, Phys. Rev. Lett. **82**, 5229 (1999).
[5] D. Budker, D. F. Kimball, S. M. Rochester, and V. V. Yashchuk, Phys. Rev. Lett. **83**, 1767 (1999).
[6] G. Heinze, C. Hubrich, and T. Halfmann, Phys. Rev. Lett. **111**, 033601 (2013).
[7] K. P. Heeg, J. Haber, D. Schumacher, L. Bocklage, H.-C. Wille, K. S. Schulze, R. Loetzsch, I. Uschmann, G. G. Paulus, R. Rüffer, R. Röhlsberger, and J. Evers, Phys. Rev. Lett. **114**, 203601 (2015).
[8] C. Liu, Z. Dutton, C. H. Behroozi, and L. V. Hau, Nature **409**, 490 (2001).
[9] D. F. Phillips, A. Fleischhauer, A. Mair, R. L. Walsworth, and M. D. Lukin, Phys. Rev. Lett. **86**, 783 (2001).
[10] T. N. Dey and G. S. Agarwal, Phys. Rev. A **67**, 033813 (2003).
[11] M. Fleischhauer and M. D. Lukin, Phys. Rev. Lett. **84**, 5094 (2000).
[12] A. André and M. D. Lukin, Phys. Rev. Lett. **89**, 143602 (2002).
[13] M. Bajcsy, A. S. Zibrov, and M. D. Lukin, Nature **426**, 638 (2003).
[14] F. E. Zimmer, A. André, M. D. Lukin, and M. Fleischhauer, Opt. Commun. **264**, 441 (2006).
[15] F. E. Zimmer, J. Otterbach, R. G. Unanyan, B. W. Shore, and M. Fleischhauer, Phys. Rev. A **77**, 063823 (2008).
[16] S. A. Moiseev and B. S. Ham, Phys. Rev. A **71**, 053802 (2005).
[17] S. A. Moiseev and B. S. Ham, Phys. Rev. A **73**, 033812 (2006).
[18] Y.-W. Lin, W.-T. Liao, T. Peters, H.-C. Chou, J.-S. Wang, H.-W. Cho, P.-C. Kuan, and I. A. Yu, Phys. Rev. Lett. **102**, 213601 (2009).
[19] G. Nikoghosyan and M. Fleischhauer, Phys. Rev. A **80**, 013818 (2009).
[20] M. Fleischhauer, J. Otterbach, and R. G. Unanyan, Phys. Rev. Lett. **101**, 163601 (2008).
[21] M. Kiffner and M. J. Hartmann, Phys. Rev. A **82**, 033813 (2010).
[22] S. E.Harris, J. E. Field, A. Imamoglu, Phys. Rev. Lett. **64**, 1107 (1990).
[23] H. Wang, D. Goorskey and M. Xiao, Phys. Rev. Lett. **87**, 073601 (2001).
[24] J. P. Marangos, J. Mod. Opt. **45**, 471 (1998).
[25] R. Fleischhaker and J. Evers, Phys. Rev. A **77**, 043805 (2008).
[26] H. Schmidt and A. Imamŏglu, Opt. Lett. **21**, 1936 (1996).
[27] H. Kang and Y. Zhu, Phys. Rev. Lett. **91**, 093601 (2003).
[28] G. F. Sinclair and N. Korolkova, Phys. Rev. A **76**, 033803 (2007).
[29] J. H. Li, X. Y. Lu, J. M. Luo, and Q. J. Huang, Phys. Rev. A **74**, 035801 (2006).
[30] J. Sheng, X. Yang, U. Khadka and M. Xiao, Opt. Exp. **19**, 17059 (2011).
[31] M. Bajcsy, S. Hofferberth, V. Balic, T. Peyronel, M. Hafezi, A. S. Zibrov, V. Vuletic, and M. D. Lukin, Phys. Rev. Lett. **102**, 203902 (2009).

[32] M. Kiffner and M. J. Hartmann, Phys. Rev. A **81**, 021806(R) (2010).
[33] M. Hafezi, D. E. Chang, V. Gritsev, E. A. Demler and M. D. Lukin, EPL **94**, 54006 (2011).
[34] D. E. Chang, V. Gritsev, G. Morigi, V. Vuletic, M. D. Lukin, and E. A. Demler, Nat. Phys. **4**, 884 (2008).
[35] A. Andre, M. Bajcsy, A. S. Zibrov, and M. D. Lukin, Phys. Rev. Lett. **94**, 063902 (2005).
[36] L. E. Zohravi, M. Abedi and M. Mahmoudi, Commun. Theor. Phys. **61**, 506 (2014).
[37] T. N. Dey and G. S. Agarwal, Phys. Rev. A **76**, 015802 (2007).
[38] S. E. Harris and Y. Yamamoto, Phys. Rev. Lett. **81**, 3611 (1998).
[39] D. Maxwell, D. J. Szwer, D. Paredes-Barato, H. Busche, J. D. Pritchard, A. Gauguet, K. J. Weatherill, M. P. A. Jones, and C. S. Adams, Phys. Rev. Lett. **110**, 103001 (2013).
[40] S. Sevincli, N. Henkel, C. Ates, and T. Pohl, Phys. Rev. Lett. **107**, 153001 (2011).
[41] C. S. Hofmann, G. Günter, H. Schempp, M. Robert-de-Saint-Vincent, M. Gärttner, J. Evers, S. Whitlock, and M. Weidemüller Phys. Rev. Lett. **110**, 203601 (2013).
[42] A. V. Gorshkov, J. Otterbach, M. Fleischhauer, T. Pohl, and M. D. Lukin, Phys. Rev. Lett. **107**, 133602 (2011).
[43] G. P. Agrawal, Nonlinear Fiber Optics (Academic, Boston, 1989).
[44] M. Kiffner and K.-P. Marzlin, Phys. Rev. A **71**, 033811 (2005).
[45] M. Kiffner and U. Dorner and D. Jaksch, Phys. Rev. A **85** 023812 (2012).